南京航空航天大学

论文集

（二〇〇八年） 第3册

航空宇航学院

（第3分册）

南京航空航天大学科技部编

二〇〇九年五月

航空宇航学院

013 系

航空宇航学院2008年学术论文清单（0131）

序号	姓名	职称	单位	论文题目	刊物、会议名称	年、卷、期
1	刘 博 胡海岩	博士 教授	0131 0131	Stabilization of linear undamped systems via position and delayed position feedbacks	Journal of Sound and Vibration	2008.312.03
2	刘 博 胡海岩	博士 教授	0131 0131	滤波器群时延对受控倒立摆稳定性的影响	第八届全国动力学与控制学术会议	
3	茅晓晨 胡海岩	博士 教授	0131 0131	Stability and Hopf bifurcation of a delayed network of four neurons with a short-cut connection	International Journal of Bifurcation and Chaos	2008.18.10
4	茅晓晨 胡海岩	博士 教授	0131 0131	四神经元时滞网络的稳定性与分岔	第八届全国动力学与控制学术会议	
5	原口正和 胡海岩	博士 教授	0131 0131	Using a new discretization approach to design a delayed LQG controller	Journal of Sound and Vibration	2008.314.3-5
6	刘丽丽 文浩 金栋平 胡海岩	博士 博士 教授 教授	0131 0131 0131 0131	三体绳系卫星面内编队飞行的回收控制	振动工程学报	2008.40.03
7	文浩 金栋平 胡海岩	博士 教授 教授	0131 0131 0131	Advances in dynamics and control of tethered satellite systems	Acta Mechanica Sinica	2008.24.03
8	文浩 金栋平 胡海岩	博士 教授 教授	0131 0131 0131	Infinite-horizon control for retrieving a tethered subsatellite via an elastic tether	Journal of Guidance, Control, and Dynamics	200831.04
9	文浩 金栋平 胡海岩	博士 教授 教授	0131 0131 0131	Optimal feedback control of the deployment of a tethered subsatellite subject to perturbations	Nonlinear Dynamics	2008.51.04
10	文浩 金栋平 胡海岩	博士 教授 教授	0131 0131 0131	Three-dimensional optimal deployment of a tethered subsatellite with an elastic tether	International Journal of Computer Mathematics	2008.85.06
11	文浩 金栋平 胡海岩	博士 教授 教授	0131 0131 0131	基于微分包含的绳系卫星时间最优释放控制	力学学报	2008.40.01
12	文浩 金栋平 胡海岩	博士 教授 教授	0131 0131 0131	倾斜轨道电动力绳系卫星回收控制	力学学报	2008.40.03
13	冉玉国 韩景龙 员海玮	硕士 教授 博士后	13	间隙非线性结构气弹响应分析程序的DMAP开发	南京航空航天大学学报	2007.39.01
14	陈前 K Worden	教授 教授	0131 外单位	Properties of viscoelastic structures with time-dependent Poisson’s ratio	7th European Conference of Structural Dynamics	
15	Laith K Abbas 陈前	博士生 教授	0131 0131	Aeroelastic behaviour of lifting surfaces with freeplay and aerodynamic stiffness and damping nonlinearities	International Journal of Bifurcation and Chaos (IJBC).	2008.18.04
16	Laith K Abbas 陈前 Piergiovanni Marzocca	博士后 教授	0131 0131	Active aerothermoelastic control of hypersonic double-wedge lifting surface	Chinese Journal of Aeronautics	2008.21.01
17	Laith K Abbas 陈前 Piergiovanni Marzocca	博士后 教授	0131 0131	Non-linear aeroelastic investigations of a store (s) induced limit cycle oscillations	Journal of Aerospace Engineering.	2008.222.01
18	周宏伟 陈前	博士 教授	0131 0131	电磁颗粒阻尼器减振机理及试验研究	《振动工程学报》	2008.21.02
19	周宏伟 陈前	博士 教授	0131 0131	颗粒阻尼系统动力学特性研究	《振动与冲击》	2008.27.04
20	周宏伟 陈前	博士 教授	0131 0131	阻尼颗粒动态特性研究	《南京航空航天大学学报》	2008.21.02
21	游伟倩 陈怀海 贺旭东	博士 教授 讲师	0131 0131 0131	高阶柔性结构系统振动控制中加权函数的选择	航空学报	2008.29.2

22	何欢 陈国平 张家滨	讲师 教授	0131 0131 0131	带油箱结构的机身框段坠撞仿真分析	航空学报	2008.29.03
23	何欢 马常亮 陈国平	讲师 讲师 教授	0131 0131 0131	气囊缓冲系统在着陆回收领域中的应用	2008中国空间技术研究院科技委返回与回收专业组2008年学术交流会	
24	马常亮 何欢 陈国平	讲师 讲师 教授	0131 0131 0131	气囊着陆缓冲系统的排气孔面积优化	2008中国空间技术研究院科技委返回与回收专业组2008年学术交流会	
25	员海玮 韩景龙	博士后 教授	0131 0131	Match Point Solution for Robust Flutter Analysis in Constant-Mach Prediction	Chinese Journal of Aeronautics	2008.21.02
26	员海玮 韩景龙	博士后 教授	0131 0131	飞行高度摄动的鲁棒颤振计算方法	南京航空航天大学学报	2007.39.06
27	员海玮 韩景龙	博士后 教授	0131 0131	非线性气动弹性系统的鲁棒稳定性分析	振动工程学报	2008.21.04
28	赵晓平 张令弥 郭勤涛	博士 教授 副教授	0131 0131	基于瞬时频率估计的自适应Vold-Kalman阶比跟踪研究	振动与冲击	2008.27.12
29	赵晓平 张令弥 郭勤涛	博士 教授 副教授	0131 0131 0131	旋转机械阶比跟踪技术研究进展综述	地震工程与工程振动	2008.28.06
30	赵晓平 孔庆鹏 郭勤涛	博士 副教授 副教授	0131 0131 0131	Study of time-frequency order tracking of vibration signals of rotating machinery in changing state	2008 International Symposiums on Information Processing	2008
31	赵建洋 张令弥	博士 教授	0131 0131	基于主列筛选的动态测试传感器配置方法研究	航空学报	200829.06
32	蔡祥梅 刘先斌	学生 教授	0131 0131	白噪声参激一类余维2 分岔系统最大Lyapunov 指数研究	力 学 季 刊	2008.29.02
33	刘志军 陈国平 张 方 党志杰	学生 教授	0131 0131	超长斜拉索张力振动法测量研究	振动与冲击	2008.27.01
34	秦远田 陈国平 余 岭 张 方	学生 教授	0131 0131	车-桥耦合系统动力学建模与响应分析	应用力学学报	2008.25.01
35	邓吉宏 王轲 陈国平 张方 施荣明 陈忠明	学生 副教授	0131 0131	金属橡胶减振器用于发动机安装减振的研究	航空学报	2008.29.06
36	谢琳艳 陈国平	硕士 教授	0131 0131	封闭圆柱壳振动与内声场耦合的数值计算	江苏航空	2008.增刊
37	李为 陈国平	硕士 教授	0131 0131	含转动连接的平面梁结构连接刚度修正	江苏航空	2008.增刊
38	周忠斌 王永亮	硕士 教授	0131 0131	弹性平面问题的微分求积单元法研究	江苏航空	2008.增刊
39	杨凯 陈国平	硕士 教授	0131 0131	考虑着舰基础横摇状态下飞机着舰动力学仿真	江苏航空	2008.增刊
40	于元东 纪国宜	硕士 副研究员	0131 0131	“E型”电涡流激振器的研制	江苏航空	2008.增刊
41	王成强 陈怀海 贺旭东 姜双燕	硕士 教授	0131 0131	基于转角振型曲率的损伤识别	江苏航空	2008.增刊
42	张翠霞 陈前 腾汉东	硕士 教授	0131 0131 0131	液固混合介质缓冲器的动力学特性研究	江苏航空	2008.增刊

航空宇航学院2008年学术论文清单（0133）

序号	姓名	职称	单位	论文题目	刊物、会议名称	年、卷、期
1	陈怀壮 邓宗白	硕士 教授	0133 0133	基于PATRAN的推力矢量导流管的设计研究	飞机工程	2007.04
2	胡玉琴 邓宗白	硕士 教授	0133 0133	浅析扭转理论的发展	力学与实践	2008.30.04
3	陈建平 陶秋帆 袁健	副教授 副教授 副教授	0133 0133 0133	荡秋千动力学过程的数值模拟	力学与实践	2008.30.02
4	唐静静 范钦珊	讲师 教授	0133 0133	基础力学课程研究型教学方法的探索	力学与实践	2008.30.04
5	王立峰 K.M. Liew Xiaoqiao He Yangao Hu Q. Wang 郭万林 胡海岩	教授	0133	Using Model of Strain Gradient Membrane Shell to Characterize Longitudinal Wave Dispersion in Multi-Walled Carbon Nanotubes	Journal of Computational and Theoretical Nanoscience	2008.05.10
6	王立峰 郭万林 胡海岩	教授	0133 外单位 0131	Group velocity of wave propagation in carbon nanotubes	Proceedings of Royal Society A	2008.464.2094
7	张羽鹏 王开福	硕士 教授	0133 0133	红外技术在测速中的应用	红外技术	2008.30.11
8	张明 胡明敏	副教授 教授	0133 0133	新型数字疲劳传感器设计	传感器与微系统	2008.27.08
9	张明 胡明敏 李训涛	副教授 教授 初级	0133 0133 0133	基于疲劳传感器的桥梁载荷谱检测研究	力学季刊	2007.28.4
10	张明 姚恩涛 张军 董静怡 刘海青	副教授 教授	0133 0133 033 033 033	基于电容传感器的围护结构含水率层析方法	传感器与微系统	2008.27.10
11	纪丕华 胡明敏	硕士 教授	0133 0133	光纤埋入CFPR后的试验和ANSYS分析研究	中国制造业信息化	2008.37.23
12	纪丕华 胡明敏	硕士 教授	0133 0133	基于ANSYS的CFPD屈曲分析研究	机械	2008.35.09
13	纪丕华 胡明敏	硕士 教授	0133 0133	数字疲劳传感器的设计及应用	理化检验物理分册	2008.44.10
14	厉成元 胡明敏	硕士 教授	0133 0133	基于C++Builder的串口通讯	2008年第一届全国微电子计量测试学术研讨会	2008
15	孙伟 何小元 C.Quan	讲师 教授 副教授	0133 外单位 外单位	非单调条纹图的相位恢复新方法	光学学报	2008.28.05
16	孙伟 何小元 C.Quan 郑翔	讲师 教授 副教授 副教授	0133 外单位 外单位 外单位	基于数字图像相关的三维刚体位移测量方法研究	光学学报	2008.28.05
17	孙伟 何小元 郑翔	讲师 教授 副教授	0133 外单位 外单位	基于单摄像机的三维位移测试方法	光学学报	2008.28.09
18	刘荣梅	讲师	0133	基于疲劳传感器的大型桥梁载荷谱检测研究	实验力学	2008.23.01
19	刘荣梅 胡明敏 李训涛	讲师 教授 初级	0133 0133 0133	新型疲劳传感器设计与性能研究	传感器与微系统	2008.27.06
20	王桂娜 苏小光	硕士 教授	0133 0133	比例阀性能智能测试系统的研究	传感器与微系统	2008.27.02

21	王杰 苏小光	硕士 教授	0133 0133	基于嵌入式Web技术的自动配气系统的设计	电子测量技术	2008.31.07
22	李训涛 胡明敏 纪？华	初级 教授 硕士	0133 0133 0133	疲劳传感器标定装置的研制	实验技术与管理	2008.25.08
23	吕欣 袁健	硕士 副教授	0133 0133	基于LC理论和概率神经网络的损伤识别	江苏航空	2008.增刊
24	孙乐 胡明敏	硕士 副教授	0133 0133	基于数字疲劳传感器的桥梁载荷谱研究	江苏航空	2008.增刊
25	杨仕福 王立峰 赵永辉	硕士 教授	0133 0133	分段线性气动弹性系统的作动器饱和控制率研究	江苏航空	2008.增刊
26	娄锐 陈建平 虞伟建	硕士	0133 0133 0133	考虑机翼柔性的起落架动力学建模与仿真	江苏航空	2008.增刊

Available online at www.sciencedirect.com
ScienceDirect
Journal of Sound and Vibration 316 (2008) 122–136
JOURNAL OF SOUND AND VIBRATION
www.elsevier.com/locate/jsvi

Reconstruction of distributed dynamic loads on an Euler beam via mode-selection and consistent spatial expression

X.Q. Jiang, H.Y. Hu*

MOE Key Laboratory of Structure Mechanics and Control for Aircraft, Nanjing University of Aeronautics and Astronautics, 210016 Nanjing, China

Received 6 October 2007; received in revised form 18 February 2008; accepted 20 February 2008
Handling Editor: J. Lam
Available online 3 April 2008

Abstract

The paper presents a new approach to reconstruct the distributed dynamic loads on an Euler beam from the beam response. The approach is based on a mode-selection method and an idea of consistent spatial expression for the distributed dynamic loads, and is supported by error estimation. The idea of the optimal range of frequency and spatial modes for load reconstruction is proposed and verified by numerical simulations. To cope with the tough problem of identifying the dynamic loads near a fixed boundary, the concept of consistent spatial expression for the dynamic loads is put forward, and the Legendre polynomials are used as the consistent orthogonal base functions to describe the distributed dynamic loads. The numerical simulations show that the reconstruction accuracy near the fixed boundaries can be greatly enhanced.

1. Introduction

The identification of dynamic loads on a structure is of great practical interest in aerospace engineering, mechanical engineering, civil engineering and so on because a prior knowledge of the dynamic loads is essential for the design, analysis and evaluation of the structure, while the direct measurements of dynamic loads are often not feasible in practice. The past decade has witnessed numerous studies of identifying the dynamic loads on a system of multiple degrees of freedom [1–4], the moving loads on a bridge [5,6], and impulsive load or multi-point load on a continuum [7–9]. The identification of spatially distributed dynamic loads on a continuum is relatively new [10–14]. For instance, Liu and Shepard [11] studied the reconstruction of harmonic force applied on a beam, while Granger and Perotin [14] investigated the identification of the random excitation on a beam. In these two studies, they introduced and used similar but different ideas of modified modal expression for beam dynamics. Pezerat and Guyader [13] studied the reconstruction of harmonic excitation acting on a rectangular plate, and Djamaa et al. [10] studied the load on a thin cylindrical shell. In both studies, they used the model of finite elements to describe the plate and the shell. Furthermore,

*Corresponding author. Tel.: +86 25 8489 1672; fax: +86 25 8489 1512.
E-mail address: hyhu@nuaa.edu.cn (H.Y. Hu).

0022-460X/$ - see front matter © 2008 Elsevier Ltd. All rights reserved.
doi:10.1016/j.jsv.2008.02.038

Sehlstedt [12] investigated a seemingly different problem to reconstruct the boundary traction on a constrained structure.

The reconstruction of distributed dynamic loads on a continuum is a complex inverse problem with inherent ill-posedness. However, it is not clear whether the ill-posedness results from physics or mathematics. In engineering practice, to reconstruct the distributed dynamic loads on a continuum is an expansive mapping process of deducing continuous integrated load information from discrete parts of response information, which makes the problem so involved that many aspects have to be dealt with. In the studies mentioned above and some others, much attention was paid to the complicated technical problems in mathematics, especially in the ill-posedness and regularization methods [15–22], while less consideration was put to the physical nature of the problem.

This paper is mainly concerned with some physical aspects of the identification of distributed dynamic loads. For example, attention will be paid to whether or not the distributed dynamic loads on a continuum can be reconstructed integrally from the response data by inverse inference. A reasonable extension of this question is that the reconstruction of distributed dynamic loads can be made only in part. From the viewpoint of the forward problem from the dynamic load to the dynamic response, the continuum acts as a transducer with the inherent physical property of smoothness. That is, the continuum behaves like an inverse transducer that enlarges the unevenness in response information. Thus, the continuum as an inverse transducer is naturally ill-posed in physics, instead of in mathematics only. In addition, attention will be paid to the following questions. Will the above fact suggest that the reconstruction of distributed dynamic loads on a continuum can be solved only in part? To what degree can the result of the reconstruction be controlled? Will it be different when a strategy intending in advance to obtain only some limited range of the load information is adopted?

In practice, the measurements of dynamic response are often not enough for the reconstruction of dynamic loads. Consequently, many studies have focused on the additional information. However, it does not seem an efficient policy. In this study, an idea of drawing the inner relation between the temporal and spatial information from the measurements will be considered so as to establish a strong linkage between the temporal response data and the spatial response data, since they are through the same system and are parts of the integrated response information.

For simplicity, this study will focus on the reconstruction of the dynamic loads on an undamped Euler beam so as to clarify some phenomena in the inverse problem of reconstructing distributed dynamic loads on a continuum from discrete response data. The rest of the paper is organized as follows. In Section 2, a concept of "scale effect" is first proposed to reveal the relation between the temporal and spatial information in the beam response, and then it is applied to the "mode selection" approach to determine the appropriate range for the load reconstruction with acceptable accuracy. In the previous studies of reconstructing the dynamic loads on a beam [11,14], the modified modal functions were employed to describe the distributed dynamic loads. With regard to simply supported boundary conditions, the modal functions, including the modified modal functions, gradually tend to be zero near the fixed boundary and conflict with the dynamic loads not vanishing near the fixed boundary. In Section 3, therefore, a concept of "consistent spatial expression for distributed dynamic loads" is suggested to cope with the boundary problem. In Section 4, several numerical simulations will be given to demonstrate the theoretical results in Sections 2 and 3. Finally, some concluding remarks are made in Section 5.

2. Mode selection

The dynamic response of a uniform undamped Euler beam yields a dimensionless partial differential equation as follows:

$$\frac{(\kappa_1 L)^4}{4\pi^2}\frac{\partial^2 \bar{w}(\bar{x},\bar{t})}{\partial \bar{t}^2}+\frac{\partial^4 \bar{w}(\bar{x},\bar{t})}{\partial \bar{x}^4}=\bar{f}(\bar{x},\bar{t}), \tag{1}$$

where $\bar{x}\equiv x/L$ is the dimensionless spatial variable scaled by the length L of beam, $\bar{t}\equiv t/T_1$ the dimensionless time scaled by $T_1\equiv 2\pi/\omega_1$, $\omega_1\equiv\kappa_1^2\sqrt{EI/\rho A}$, $\bar{w}\equiv w/L$ the dimensionless translational displacement, $\bar{f}\equiv L^3 f/(EI)$ the dimensionless external transverse excitation, κ_1 the circular wavenumber of the first modal

shape, ρ the density of beam material, E the Young's modulus of beam material, A the area of cross section of beam, and I the second moment of the area, respectively.

With the use of modal transformation $\bar{w}(\bar{x},\bar{t}) = \sum_{m=1}^{\infty} W_m(\bar{x})q_m(\bar{t})$, the mth modal response corresponding to Eq. (1) becomes

$$\ddot{q}_m(\bar{t}) + \bar{\omega}_m^2 q_m(\bar{t}) = \frac{4\pi^2}{(\kappa_1 L)^4}\bar{f}_m(t), \tag{2}$$

where the dot represents the derivative with respect to the dimensionless time $\bar{t}$, $q_m(\bar{t})$ is the modal coordinate, $\bar{f}_m(\bar{t}) \equiv \int_0^1 W_m(\bar{x})\bar{f}(\bar{x},\bar{t})\,\mathrm{d}\bar{x}$ the general force, and $W_m(\bar{x})$ the mode shape, respectively.

If the transverse excitation is harmonic in the time domain and proportional to the jth mode shape in the spatial domain, namely

$$\bar{f}(\bar{x},\bar{t}) = cW_j(\bar{x})\mathrm{e}^{\mathrm{i}\bar{\omega}\bar{t}}, \tag{3}$$

where c is a positive real constant, the general force and the corresponding steady-state response of the mth mode read

$$\bar{f}_m(\bar{t}) = c\delta_{jm}\mathrm{e}^{\mathrm{i}\bar{\omega}\bar{t}}, \tag{4}$$

$$q_m(\bar{t}) = c\frac{4\pi^2}{(\kappa_1 L)^4}\delta_{jm}\frac{1}{\bar{\omega}_m^2 - \bar{\omega}^2}\mathrm{e}^{\mathrm{i}\bar{\omega}\bar{t}}, \quad \ddot{q}_m(\bar{t}) = c\frac{4\pi^2}{(\kappa_1 L)^4}\delta_{jm}\frac{1}{1-(\bar{\omega}_m/\bar{\omega})^2}\mathrm{e}^{\mathrm{i}\bar{\omega}\bar{t}}, \tag{5}$$

where δ_{jm} is the Kronecker delta.

To check the scale effect of the variance of both mode order m and excitation frequency $\bar{\omega}$, it is useful to introduce two factors as follows:

$$\mathrm{SF}_{\bar{w}} \equiv \frac{1}{\bar{\omega}_m^2 - \bar{\omega}^2}, \quad \mathrm{SF}_{\bar{a}} \equiv \frac{1}{1-(\bar{\omega}_m/\bar{\omega})^2}. \tag{6}$$

With the help of $\mathrm{SF}_{\bar{w}}$ and $\mathrm{SF}_{\bar{a}}$, the translational displacement and acceleration of the steady-state response can be expressed as

$$\bar{w}(\bar{x},\bar{t}) = c\frac{4\pi^2}{(\kappa_1 L)^4}\mathrm{SF}_{\bar{w}}W_j(\bar{x})\mathrm{e}^{\mathrm{i}\bar{\omega}\bar{t}}, \quad \bar{a}(\bar{x},\bar{t}) = c\frac{4\pi^2}{(\kappa_1 L)^4}\mathrm{SF}_{\bar{a}}W_j(\bar{x})\mathrm{e}^{\mathrm{i}\bar{\omega}\bar{t}}. \tag{7}$$

For a simply supported Euler beam, $(\kappa_1 L)^4/(4\pi^2) = \pi^2/4$, and the dimensionless circular wavenumber, circular frequency and modal shape of the mth mode are $\bar{\kappa}_m = m\pi$, $\bar{\omega}_m = 2m^2\pi$, and $W_m(\bar{x}) = \sqrt{2}\sin(\bar{\kappa}_m\bar{x})$, respectively. For the excitation frequency $\bar{\omega}$ between two natural frequencies $\bar{\omega}_k$ and $\bar{\omega}_{k+1}$, where $\bar{\omega}_0$ is defined as $\bar{\omega}_0 \equiv 0$, let $\bar{\omega} = \bar{\omega}_k + \Delta\bar{\omega}_k$ and $\Delta\bar{\omega}_k > 0$. Then, it is easy to recast Eq. (6) as

$$\mathrm{SF}_{\bar{w}} = \frac{1}{4\pi^2}\frac{1}{(k^2+\beta)^2}\frac{1}{\gamma^2-1}, \quad \mathrm{SF}_{\bar{a}} = \frac{1}{1-\gamma^2}, \tag{8}$$

where

$$\beta \equiv \frac{\Delta\bar{\omega}_k}{\bar{\omega}_1}, \quad \gamma \equiv \frac{\bar{\omega}_m}{\bar{\omega}} = \frac{m^2}{k^2+\beta}, \quad 0<\beta<2k+1. \tag{9}$$

Eq. (8) indicates that the scale effect mainly comes from $c_s \equiv 1/|1-\gamma^2|$, $\gamma \in (0,\infty)$, which is shown in Fig. 1.

Now it is clear that an undamped Euler beam is a low-pass filter in the frequency domain and the modal domain, as may be observed in Eqs. (8) and (9) from the fact that $\mathrm{SF}_{\bar{w}} \to 0$ when $k \to \infty$ but m is fixed, and that $\mathrm{SF}_{\bar{w}} \to 0$ and $\mathrm{SF}_{\bar{a}} \to 0$ when $m \to \infty$ but k and β are fixed. Furthermore, the steady-state response greatly depends on the difference between the excitation frequency and the natural frequencies corresponding to the modal components included in the spatial expression of the excitation. For example, given the harmonic excitation distributed proportionally to a mode shape in the spatial domain, the beam response becomes remarkable if the excitation frequency is close to the natural frequency corresponding to the mode shape. Otherwise, the beam response is imperceptible.

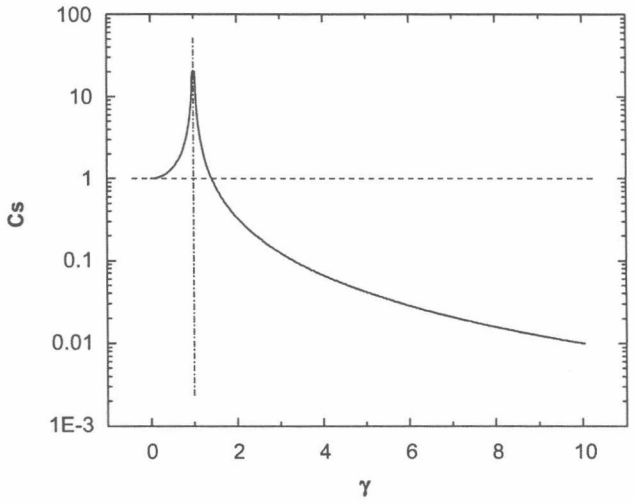

Fig. 1. Cs vs γ.

The reconstruction of distributed dynamic loads on an Euler beam is inherently a process of partial identification when any truncated modal expression is used to describe the beam response. This assertion also holds true for the reconstruction of distributed dynamic loads on any continuum. Hence, the difficulty in reconstructing the dynamic load of high frequency has been well acknowledged. Furthermore, the reconstruction of distributed dynamic loads can only be made in part since the spatial modal components of high wavenumbers have to be truncated according to the above discussion. The above facts lead to a *hypothesis* for the reconstruction of distributed dynamic loads as follows. Only the distributed dynamic loads of a certain range of frequency and spatial modes could be reconstructed from the response data, and there is an optimal range for the reconstruction when a particular level of sensitivity and noise in response measurement is given for a specific beam. Furthermore, the coincidence is that this is analogous to the function of animal's ears, which means different animals have different ranges of sound perception in nature.

Based on this hypothesis, a method named "mode selection" is proposed based on the concept of "scale factor" in Eq. (6) to determine an appropriate range for load reconstruction. When the main frequencies of loads are obtained from the response, the scale factor $SF_{\bar{w}}$ or $SF_{\bar{a}}$ of every mode can be determined, and only those modes, whose corresponding scale factors divided by the maximum scale factor are larger than a threshold, will be chosen for load reconstruction. Section 4 will demonstrate how to determine such a threshold through empirical data in simulations.

This approach seems similar to the regularization method of discarding smaller singular values, but they are not the same concept in fact. When the regularization method is tried to be applied to the process of mode selection, the results are not so good. Furthermore, though the scale effect seems apparent in the forward problem and causes no trouble, it is not the case in the inverse process. This scale effect results in ill-posedness and irreversibility in the inverse problem.

Section 4 gives some numerical simulations to verify the hypothesis. It is hard to depict the cases of the failure to reconstruct the spatial modal components of high wavenumber. However, the numerical results in Section 4 through case studies 1 and 2 show that the reconstruction accuracy is enhanced when an appropriate range is selected. The results there indicate that it is very important to determine an appropriate range of frequency and spatial modes in the load reconstruction, and that the accuracy of reconstructed load greatly decreases if the range is too broad.

3. Reconstruction of distributed dynamic loads and error analysis

Based on the hypothesis stated in Section 2, an improved theory with the help of "mode selection" will be developed in Section 3.1 to reconstruct the distributed dynamic loads on an Euler beam. Furthermore, the

theory, combined with the "consistent spatial expression" for distributed dynamic loads, is used to cope with the tough problem of identifying the distributed dynamic loads near any fixed boundary in Section 3.2. Later, the error evolution of the theory is discussed at length in Section 3.3.

3.1. Theory of the reconstruction of distributed dynamic loads

This subsection deals with the reconstruction of the distributed dynamic loads on a uniform undamped Euler beam governed by Eq. (1). If the dynamic load comprises N_p frequency components in the time domain, it can be expressed as

$$\bar{f}(\bar{x},\bar{t}) = \sum_{r=1}^{N_p} F_r(\bar{x}) e^{i\bar{\omega}_r^* \bar{t}}. \tag{10}$$

The general force and the corresponding steady-state response of the mth mode read

$$\bar{f}_m(\bar{t}) = \sum_{r=1}^{N_p} \int_0^1 W_m(\bar{x}) F_r(\bar{x})\, d\bar{x} e^{i\bar{\omega}_r^* \bar{t}} \tag{11}$$

$$q_m(\bar{t}) = \frac{4\pi^2}{(\kappa_1 L)^4} \sum_{r=1}^{N_p} \frac{1}{\bar{\omega}_m^2 - \bar{\omega}_r^{*2}} \int_0^1 W_m(\bar{x}) F_r(\bar{x}) d\bar{x} e^{i\bar{\omega}_r^* \bar{t}}, \tag{12a}$$

$$\ddot{q}_m(\bar{t}) = \frac{4\pi^2}{(\kappa_1 L)^4} \sum_{r=1}^{N_p} \frac{1}{1 - (\bar{\omega}_m/\bar{\omega}_r^*)^2} \int_0^1 W_m(\bar{x}) F_r(\bar{x})\, d\bar{x} e^{i\bar{\omega}_r^* \bar{t}} \tag{12b}$$

There follows the translational displacement and acceleration of the steady-state response:

$$\bar{w}(\bar{x},\bar{t}) = \sum_{m=1}^{\infty} W_m(\bar{x}) q_m(\bar{t}) = \frac{4\pi^2}{(\kappa_1 L)^4} \sum_{m=1}^{\infty} \sum_{r=1}^{N_p} \frac{1}{\bar{\omega}_m^2 - \bar{\omega}_r^{*2}} \int_0^1 W_m(\bar{x}) F_r(\bar{x}) d\bar{x} W_m(\bar{x}) e^{i\bar{\omega}_r^* \bar{t}}, \tag{13a}$$

$$\bar{a}(\bar{x},\bar{t}) = \sum_{m=1}^{\infty} W_m(\bar{x}) \ddot{q}_m(\bar{t}) = \frac{4\pi^2}{(\kappa_1 L)^4} \sum_{m=1}^{\infty} \sum_{r=1}^{N_p} \frac{1}{1 - (\bar{\omega}_m/\bar{\omega}_r^*)^2} \int_0^1 W_m(\bar{x}) F_r(\bar{x})\, d\bar{x} W_m(\bar{x}) e^{i\bar{\omega}_r^* \bar{t}}. \tag{13b}$$

As in Eq. (6), two factors can be introduced as follows:

$$\mathrm{SF}_{\bar{w}}(m,r) = \frac{1}{\bar{\omega}_m^2 - \bar{\omega}_r^{*2}}, \quad \mathrm{SF}_{\bar{a}}(m,r) = \frac{1}{1 - (\bar{\omega}_m/\bar{\omega}_r^*)^2}. \tag{14}$$

To separate the spatial and temporal information from the beam response, it is useful to introduce several abbreviation notations as follows:

$$\bar{c}_{mr} = \int_0^1 W_m(\bar{x}) F_r(\bar{x})\, d\bar{x}, \tag{15}$$

$$\bar{g}_r^{\bar{w}}(\bar{x}) = \sum_{m=1}^{\infty} \bar{c}_{mr} \mathrm{SF}_{\bar{w}}(m,r) W_m(\bar{x}), \quad \bar{g}_r^{\bar{a}}(\bar{x}) = \sum_{m=1}^{\infty} \bar{c}_{mr} \mathrm{SF}_{\bar{a}}(m,r) W_m(\bar{x}). \tag{16}$$

With the help of the above notations, it is easy to recast Eq. (13) as

$$\bar{w}(\bar{x},\bar{t}) = \frac{4\pi^2}{(\kappa_1 L)^4} \sum_{r=1}^{N_p} \bar{g}_r^{\bar{w}}(\bar{x}) e^{i\bar{\omega}_r^* \bar{t}}, \quad \bar{a}(\bar{x},\bar{t}) = \frac{4\pi^2}{(\kappa_1 L)^4} \sum_{r=1}^{N_p} \bar{g}_r^{\bar{a}}(\bar{x}) e^{i\bar{\omega}_r^* \bar{t}}. \tag{17}$$

The reconstruction of the distributed dynamic loads from the beam response begins with the measured translational displacements denoted as

$$\bar{w}(\bar{x}_i,\bar{t}_n), \quad i = 1,\ldots,N_m, \quad n = 1,\ldots,N_T, \tag{18}$$

where N_m is the number of measurement locations along the beam and N_T the number of data in time dimension. From a simple frequency analysis, one reaches the dominate circular frequencies and the corresponding amplitudes contained in the response data denoted by

$$\bar{\omega}_r^*, \quad r = 1, \ldots, N_p, \quad \bar{g}_r^{\bar{w}}(x_i), \quad r = 1, \ldots, N_p, \quad i = 1, \ldots, N_m, \tag{19}$$

where N_p is the number of dominate frequencies, and $\bar{\omega}_r^*$ is sorted so that $\bar{\omega}_1^* < \cdots < \bar{\omega}_{N_p}^*$. The amplitude corresponding to the rth dominate circular frequency $\bar{\omega}_r^*$ yields

$$\bar{g}_r^{\bar{w}}(\bar{x}_i) = \sum_{m=1}^{\infty} \bar{c}_{mr} \mathrm{SF}_{\bar{w}}(m, r) W_m(\bar{x}_i), \quad i = 1, \ldots, N_m. \tag{20}$$

Now that the sets of $\bar{\omega}_r^*$ and $\bar{g}_r^{\bar{w}}(\bar{x}_i)$ are available, the scale factors $\mathrm{SF}_{\bar{w}}$ and $\mathrm{SF}_{\bar{a}}$ can be calculated, the limitation of the magnitude level of $\bar{c}_{mr}$ can be estimated, and the modes can be selected and denoted as a set B_m. If the number of modes in B_m is M, Eq. (20) can practically be given as a truncated form as follows:

$$\bar{g}_r^{\bar{w}}(\bar{x}_i) = \sum_{m \in B_m} \bar{c}_{mr} \mathrm{SF}_{\bar{w}}(m, r) W_m(\bar{x}_i), \quad i = 1, \ldots, N_m. \tag{21}$$

Eq. (21) may be an ill-posed problem for the solution of $\bar{c}_{mr}$. Consequently, the pseudo-inverse method or regularization approach, such as Tikhonov regularization [16,20,23], should be employed. When $\bar{c}_{mr}$ is solved from Eq. (21), the remaining problem is solving Eq. (15) for $F_r(\bar{x})$. Eq. (15) can be regarded as a mapping A from the space of all kinds of $F_r(\bar{x})$, denoted as U, to the space of all $W_m(\bar{x})$, denoted as V. That is, $A: U \to V$. Hence, Eq. (15) can be solved for $F_r(\bar{x})$ by using the projection method as below [24].

Let U_N be an N-dimensional subspace of U with a series of orthogonal base functions $\{\varphi_n(\bar{x})\}$ with respect to a given inner product, V_M be an M-dimensional subspace of V with a series of orthogonal base functions $\{W_m(\bar{x})\}$ having the inner product defined by $\langle W_i, W_j \rangle = \int_0^1 W_i(\bar{x}) W_j(\bar{x}) \, \mathrm{d}\bar{x}$, and the following relations hold:

$$U_N \subset U_{N+1} \subset \cdots \subset U, \quad V_M \subset V_{M+1} \subset \cdots \subset V. \tag{22}$$

The definition of a projection operator $Q_M: V \to V_M$ enables one to establish an approximate projection

$$Q_M A|_{U_N} : U_N \to V_M. \tag{23}$$

Therefore, Eq. (15) as an approximate projection (23) can easily be recast as the following matrix equation:

$$\bar{\mathbf{A}}\,\mathbf{a} = \bar{\mathbf{c}}, \tag{24}$$

where $\bar{\mathbf{A}} \equiv [\int_0^1 W_m(\bar{x}) \varphi_n(\bar{x}) \, \mathrm{d}\bar{x}]_{M \times N}$, $\bar{\mathbf{c}} \equiv \{\bar{c}_{mr}\}_{M \times 1}$, and $\mathbf{a} \equiv \{a_n\}_{N \times 1}$ are the coefficients in expression $F_r(\bar{x}) = \sum_{\varphi_n \in U_n} a_n \varphi_n(\bar{x})$. Solving Eq. (24) for $\mathbf{a}$ gives $F_r(\bar{x})$ through the following truncated expansion:

$$F_r(\bar{x}) = \sum_{\varphi_n \in U_n} a_n \varphi_n(\bar{x}). \tag{25}$$

3.2. Consistent spatial expression for distributed dynamic loads

In previous studies [11,14], as mentioned in the introduction, the modified modal functions were employed as base functions in order to describe the distributed dynamic loads on a structure as a truncated linear combination of base functions. Such a description, however, may conflict with the actual dynamic loads near the fixed boundaries of the structure. For example, either the modal functions or the modified modal functions of a beam always tend to be zero near any fixed boundary even though the dynamic loads on the beam may not vanish. Hence, it is impossible to use any linear combination of those base functions to describe the non-zero dynamic loads near the fixed boundary of a structure.

This study, therefore, explores the consistent spatial expression for distributed dynamic loads to cope with the problem. In fact, there are a great variety of base functions, such as orthogonal polynomials, for this purpose. The practice of authors indicates that the Legendre polynomials can offer a consistent spatial expression to describe the distributed dynamic loads.

3.3. Error evolution

The analysis of error evolution of the theory will follow the development of the reconstruction theory addressed in Section 3.1.

Let $\Delta\bar{w}(\bar{x}_i,\bar{t}_n)$ be the error in the experimental data $\bar{w}(\bar{x}_i,\bar{t}_n)$, $\Delta\bar{\omega}_r^*$ and $\Delta\bar{g}_r^{\bar{w}}(\bar{x}_i)$ be the errors corresponding to $\bar{\omega}_r^*$ and $\bar{g}_r^{\bar{w}}(\bar{x}_i)$ obtained from $\bar{w}(\bar{x}_i,\bar{t}_n)$ by using frequency analysis. As Eq. (21) is a truncated form, let $\Delta\tilde{g}_r^{\bar{w}}(\bar{x}_i)$ be the theoretical errors in $\bar{g}_r^{\bar{w}}(\bar{x}_i)$, and $\Delta\bar{g}_r^{\bar{w}}(\bar{x}_i)+\Delta\tilde{g}_r^{\bar{w}}(\bar{x}_i)$ be the resultant errors in $\bar{g}_r^{\bar{w}}(\bar{x}_i)$. Therefore, Eq. (21) is practically recast as

$$\bar{g}_r^{\bar{w}}(\bar{x}_i)+\Delta\bar{g}_r^{\bar{w}}(\bar{x}_i)+\Delta\tilde{g}_r^{\bar{w}}(\bar{x}_i)=\sum_{m\in B_m}\bar{c}_{m\ r}^{*}SF_{\bar{w}}^{*}(m,r)W_m^{*}(\bar{x}_i),\quad i=1,\ldots,N_m, \tag{26}$$

where $\mathrm{SF}_{\bar{w}}^{*}(m,r)$ includes the error $\Delta\mathrm{SF}_{\bar{w}}(m,r)$ resulting from the errors of $\bar{\omega}_r^*$ and $\bar{\omega}_m$, $W_m^*(\bar{x}_i)$ carries with the error of $\Delta W_m(\bar{x}_i)$ resulting from the error of $W_m(\bar{x})$. Eq. (26) can be recast in a matrix form as

$$\tilde{\mathbf{T}}\,\tilde{\mathbf{c}}=\tilde{\mathbf{g}}, \tag{27}$$

where

$$\begin{aligned}&\tilde{\mathbf{T}}\equiv[\mathrm{SF}_{\bar{w}}^{*}(m,r)W_m^{*}(\bar{x}_i)]_{N_m\times M},\ \tilde{\mathbf{c}}\equiv\{\bar{c}_{mr}^{*}\}_{M\times 1},\\ &\tilde{\mathbf{g}}\equiv\{\bar{g}_r^{\bar{w}}(\bar{x}_i)+\Delta\bar{g}_r^{\bar{w}}(\bar{x}_i)+\Delta\tilde{g}_r^{\bar{w}}(\bar{x}_i)\}_{N_m\times 1},\quad i=1,\ldots,N_m,\ m\in B_m.\end{aligned} \tag{28}$$

The Tikhonov regularization approach gives the regularized solution to Eq. (27)

$$\tilde{\mathbf{c}}_\alpha=(\tilde{\mathbf{T}}^{*}\times\tilde{\mathbf{T}}+\alpha\times\mathbf{I})^{-1}\times\tilde{\mathbf{T}}^{*}\times\tilde{\mathbf{g}}, \tag{29}$$

where the asterisk denotes conjugate transpose and α is the regularization parameter.

Suppose that the errors of $\tilde{\mathbf{T}}$ and $\tilde{\mathbf{g}}$ are bounded as

$$\|\tilde{\mathbf{T}}-\mathbf{T}\|\leqslant h,\quad \|\tilde{\mathbf{g}}-\mathbf{g}\|\leqslant\delta, \tag{30}$$

where $\|\bullet\|$ represents a consistent norm. Then, the estimation of the error of $\tilde{\mathbf{c}}_\alpha$ is given by

$$\|\tilde{\mathbf{c}}_\alpha-\mathbf{c}\|\leqslant\frac{\|\mathbf{T}^{+}\|\times\|\tilde{\mathbf{g}}\|}{\sigma_{\min}}\times\alpha+\|\mathbf{T}^{+}\|\times\delta+\frac{\sqrt{5}}{2}\times\frac{h}{\alpha}\times(\delta^2+\alpha\times\|\mathbf{c}\|^2)^{1/2}, \tag{31}$$

where $\sigma_{\min}$ is the minimal eigenvalue of $\mathbf{T}^{*}\mathbf{T}$, $\tilde{\mathbf{c}}_\alpha$ the regularized solution, and $\mathbf{c}$ the theoretical solution [23]. The matrix $\mathbf{T}$ in (31) can be replaced by $\tilde{\mathbf{T}}$, with little loss of accuracy in practice.

Finally, according to the error theorem of the projection method [24], the error estimation of the solution of Eq. (24) for $\tilde{\mathbf{a}}$ is given by

$$\|\tilde{\mathbf{a}}-\mathbf{a}\|\leqslant\|\tilde{\mathbf{c}}_\alpha-\mathbf{c}\|\times\|R_N\|+\|R_NA\mathbf{a}-\mathbf{a}\|, \tag{32}$$

where $R_N\equiv(Q_MA|_{U_N})^{-1}Q_M: V\to U_N\subset U$, and $Q_MA|_{U_N}\equiv\bar{\mathbf{A}}_{M\times N}$.

4. Case studies

This section presents two case studies first to demonstrate how the "mode selection" well supports the hypothesis of the optimal range for reconstructing distributed dynamic loads, and then gives another two case studies to show the accuracy of the improved theory on reconstructing the distributed dynamic loads and the effect near the fixed boundary.

All case studies in this section deal with a simply supported undamped Euler beam with length $L=1\,\mathrm{m}$, area of cross section $A=1.2\times10^{-3}\,\mathrm{m}^2$, second moment of area of cross section $I=3.6\times10^{-9}\,\mathrm{m}^4$, Young's modulus $E=2\times10^{11}\,\mathrm{N\,m}^{-2}$, and density $\rho=7800\,\mathrm{kg\,m}^{-3}$. Other parameters in the case studies are the time interval $T=10\,\mathrm{s}$, the sampling rate $\Delta t=0.1\,\mathrm{ms}$, the number of measures, and the position of measurements $N_x=16$, $x_i=iL/17$, $i=1,\ldots,16$. Some dimensionless parameters are the time length $\bar{T}\approx137.7680$, the sampling rate $\Delta\bar{t}\approx1.4\times10^{-3}$, and the position of measurements $\bar{x}_i=i/17$, $i=1,\ldots,16$.

In the case studies, the dimensionless translational displacements of the beam were sampled from the corresponding analytical solution, and only the steady-state responses were put into use since the components

of free vibration could easily be picked out for an undamped beam. To simulate measured data, the uniformly distributed random noises were added to the natural frequencies, mode shapes, and displacements, where an additive noise level within the upper bound of $\bar{\omega}_1/1000$ was applied to the dimensionless natural frequencies, a multiplicative noise level within the upper bound of 1/50 to the dimensionless mode shapes, and a multiplicative noise level within the upper bound of 1×10^{-3} to the dimensionless translational displacements. However, no noise was applied to the dimensionless mode shapes when they were used as orthogonal base functions to reconstruct the distributed dynamic loads.

In mode selection, a threshold ε_{SF} was introduced. The modes satisfying the inequality $|SF_{\bar{w}}(m,r)|/\max_{n\in D}(|SF_{\bar{w}}(n,r)|) \geqslant \varepsilon_{SF}(r)$ were selected and denoted as a set D_m for each dominate excitation frequency, where D is a set including enough modes under consideration. Moreover, in all case studies, the relative errors were defined as the absolute errors divided by the corresponding maximum.

The first and the second case studies are to demonstrate the effect of the "mode selection". In the first case study, the Euler beam was assumed to be subject to a harmonic excitation $\bar{f}(\bar{x},\bar{t}) = \sum_{i=1,5,6,7,10} \bar{f}_i W_i(\bar{x}) \sin(\bar{\omega}^* \bar{t})$, where $\bar{\omega}^* = \bar{\omega}_3 + 0.8\,\bar{\omega}_1$, $\bar{f}_i = 1$, $i = 1,5,6,7,10$. Fig. 2 shows how the scale factors $SF_{\bar{w}}$ of the particular frequency varied with the order of the modes. The threshold ε_{SF} was empirically tried twice. At first, when ε_{SF} was set to 1×10^{-3}, the set $D_m = 1 \ldots 11$ was selected. Fig. 3 shows the corresponding reconstruction results and errors, and indicates that the set D_m of selected modes covered all

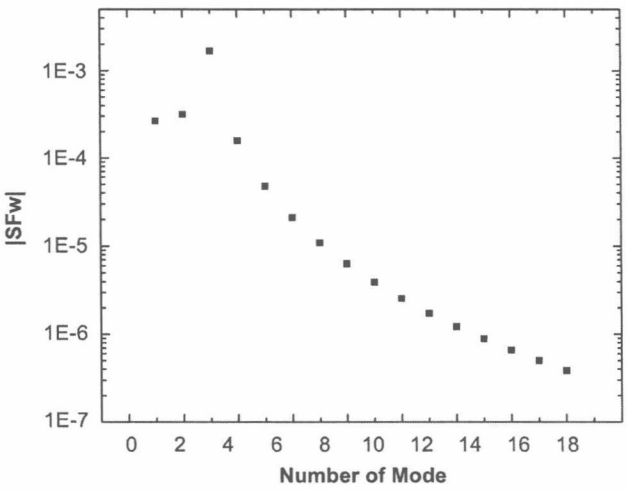

Fig. 2. $SF_{\bar{w}}$ for case 1.

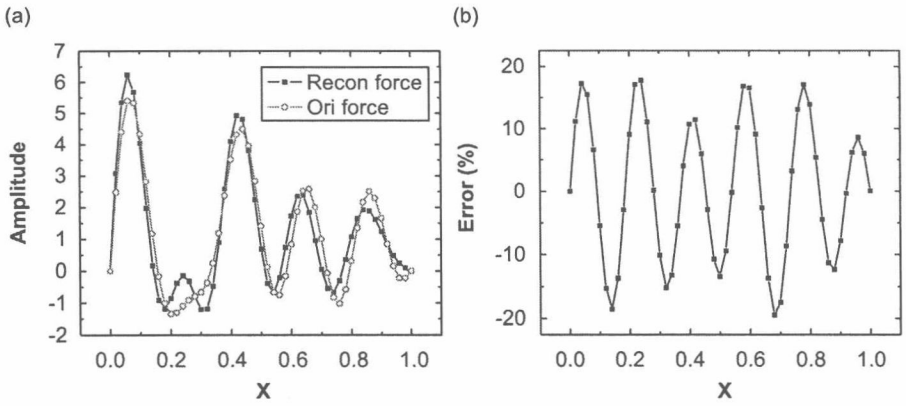

Fig. 3. Comparison between reconstructed and original loads for case 1, where $\varepsilon_{SF} = 1 \times 10^{-3}$, $D_m = 1 \ldots 11$.

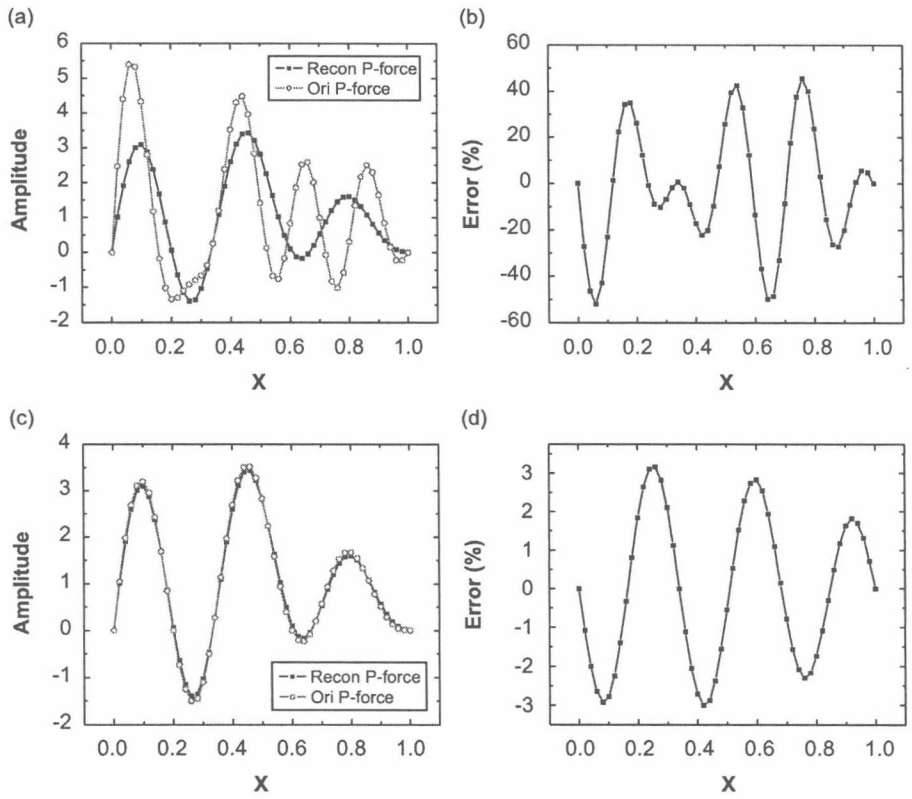

Fig. 4. Comparison between reconstructed and original loads for case 1, where $\varepsilon_{SF} = 1 \times 10^{-2}$, $D_m = 1 \ldots 6$.

spatial modes in the original load. Then, ε_{SF} was set to 1×10^{-2}, and the set $D_m = 1 \ldots 6$ was selected. In this case, D_m did not cover Modes 7 and 10 in the original load. Fig. 4 shows the reconstruction results and errors. Subfigures 4(a) and 4(b) give the comparison between the reconstructed load and the original load, whereas subfigures 4(c) and 4(d) are the comparison between the reconstructed load and the corresponding modal parts, namely, Modes 1, 5, and 6, in the original load. It is clear from Fig. 3(b) and 4(d) that the corresponding modal parts in the original load are accurately reconstructed when ε_{SF} is larger or the range of D_m is narrower. It is worthy to mention that the shapes of error curves are not important because they are influenced by the random errors.

The second case is to reconstruct the distributed dynamic loads with two harmonic components in the form $\bar{f}(\bar{x}, \bar{t}) = \sum_{i=1,5,9} \bar{f}_i W_i(\bar{x}) \sin(\bar{\omega}_1^* \bar{t}) + \sum_{j=2,6,13} \bar{f}_j W_j(\bar{x}) \sin(\bar{\omega}_2^* \bar{t})$, where $\bar{\omega}_1^* = \bar{\omega}_3 + 0.8\,\bar{\omega}_1$, $\bar{\omega}_2^* = \bar{\omega}_8 + 0.8\,\bar{\omega}_1$, and $\bar{f}_i = \bar{f}_j = 1$, $i = 1, 5, 9$, $j = 2, 6, 13$. Fig. 5 presents the variation of the scale factors $SF_{\bar{w}}$ of the two frequencies with regard to the order of the modes. Similarly, the threshold ε_{SF} was first set to 1×10^{-3}, $D_m(\bar{\omega}_1^*) = 1 \ldots 11$ and $D_m(\bar{\omega}_2^*) = 1 \ldots 16$ were selected, respectively. In this case, both sets $D_m(\bar{\omega}_1^*)$ and $D_m(\bar{\omega}_2^*)$ covered all spatial modes in the dynamic loads. Fig. 6 shows the reconstruction of the two components in (a) and (c), as well as the corresponding errors in (b) and (d). When the threshold ε_{SF} was set to 1×10^{-2}, then $D_m(\bar{\omega}_1^*) = 1 \ldots 6$ and $D_m(\bar{\omega}_2^*) = 1 \ldots 10$ were selected. The corresponding results did not cover some spatial modes in the distributed dynamic loads. Fig. 7 shows the reconstruction results and errors. Subfigures 7(a) and (b) give the comparison between the reconstructed and original loads of the first harmonic component, whereas subfigures 7(c) and (d) give the comparison between the reconstructed load and the corresponding modal parts in the original load of the first harmonic component. Subfigures 7(e) and (f) are the comparison between the reconstructed and original loads of the second harmonic component, whereas subfigures 7(g) and (h) are the comparison between the reconstructed load and the corresponding modal parts of the original load of the second harmonic component. The comparison of subfigures 7(d) and (h) to subfigures 6(b) and (d)

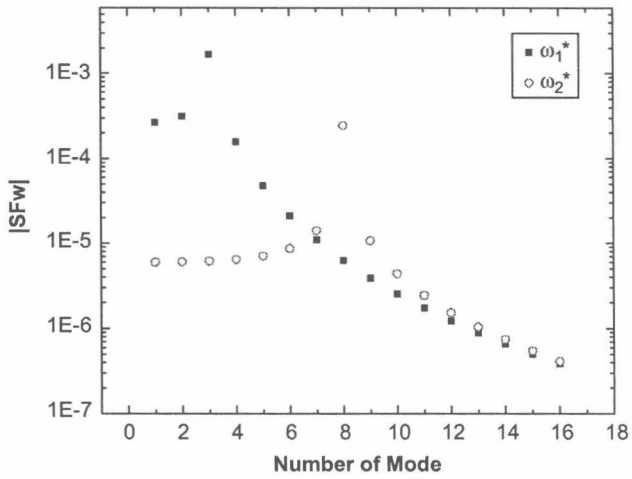

Fig. 5. $SF_{\bar{w}}$ for case 2.

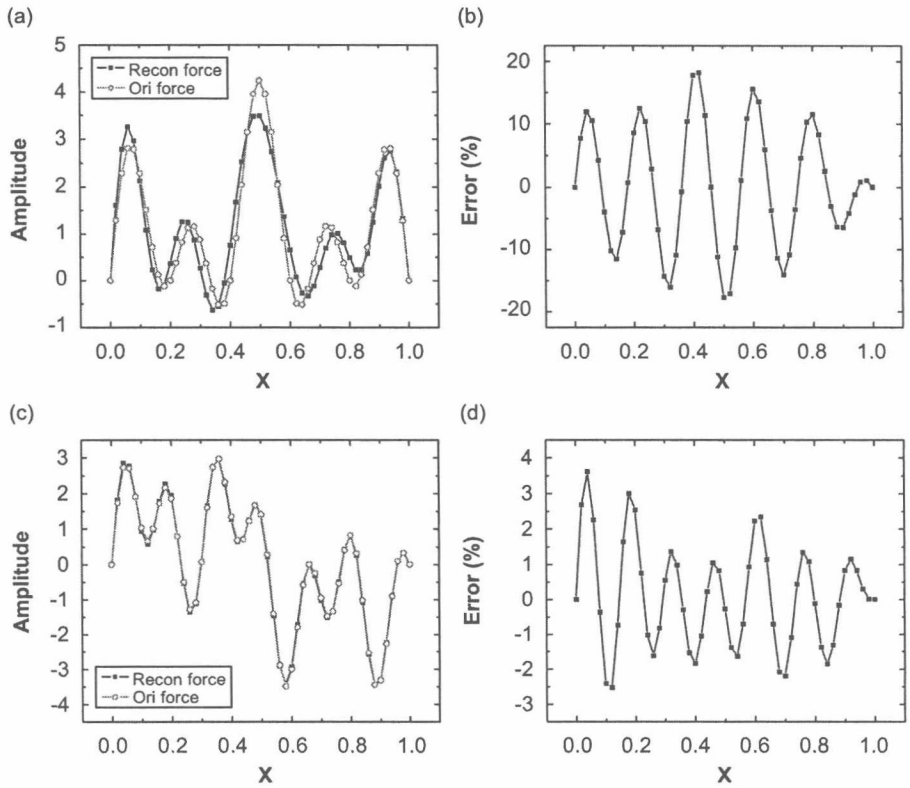

Fig. 6. Comparison between reconstructed and original loads for case 2, where $\varepsilon_{SF} = 1 \times 10^{-3}$, $D_m(\bar{\omega}_1^*) = 1 \ldots 11$, $D_m(\bar{\omega}_2^*) = 1 \ldots 16$.

indicates that a narrower range of selected modes enhances the reconstruction accuracy. However, it is not true that the narrower the range of selected modes, the higher the accuracy of the reconstruction. Therefore, an optimal range for "mode selection" is really expected.

In the above two cases $\{\varphi_n(\bar{x})\}$ were taken as the normalized natural mode functions $\{W_m(\bar{x})\}$, whereas in the following two cases $\{\varphi_n(\bar{x})\}$ were taken as the normalized modified Legendre polynomials on interval (0, 1)

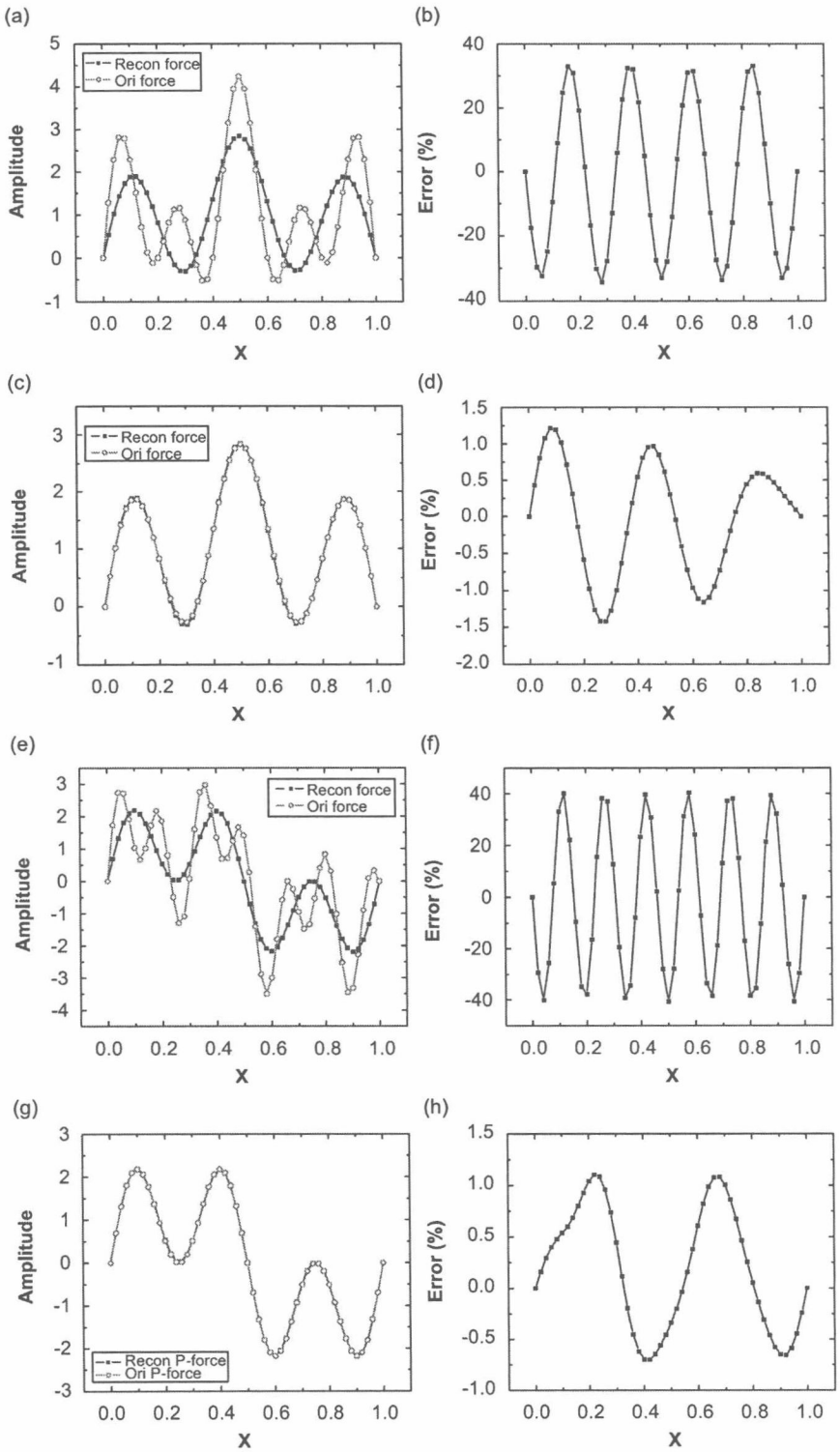

Fig. 7. Comparison between reconstructed and original loads for case 2, where $\varepsilon_{SF} = 1 \times 10^{-2}$, $D_m(\bar{\omega}_1^*) = 1 \ldots 6$, $D_m(\bar{\omega}_2^*) = 1 \ldots 10$.